Parametric Characterization of Self-Heating in Depletion-Type Si Micro-Ring Modulators

Myung Jin Shin, Yoojin Ban, Byung-Min Yu, Jinsoo Rhim, *Student Member, IEEE*, Lars Zimmermann, and Woo-Young Choi, *Member, IEEE*

***Abstract*—The influence of self-heating on the static transmission characteristics of depletion-type Si micro-ring modulators (MRMs) is investigated. Self-heating, caused by free-carrier absorption of the input light inside the doped ring waveguide, increases the effective refractive index of the ring waveguide and results in the red-shifted resonance wavelength. This phenomenon is modeled based on the coupled-mode equation with a newly-introduced self-heating coefficient *R*. The accuracy of our model is confirmed by measurement. In addition, dependence of *R* on device size and doping concentration is experimentally investigated and the resulting dependence is explained.**

***Index Terms*—Si ring modulator, self-heating coefficient, coupled-mode equation, self-heating.**

I. Introduction

OPTICAL interconnects are vigorously investigated as a solution that can overcome the electrical interconnect bottleneck problem faced by many present-day high-performance electronic systems. In particular, optical interconnect solutions based on Si photonics are attracting a great amount of research and development efforts as they can provide high-bandwidth, small-footprint, cost-effective solutions along with the possibility for easier integration with mature Si electronics [1], [2]. Since practical Si lasers are not available as of yet, Si modulators play a very important role for Si photonic interconnect systems. Among several different types of Si modulators, depletion-type Si micro-ring modulators (MRMs) based on reverse-biased p-n junctions are of great interest as they can provide high-speed operation not limited by injected carrier recombination [3], [4]. However, depletion-type Si MRMs suffer from self-heating caused by free-carrier absorption (FCA) of the input light circulating in modulator ring waveguides [5]. The ring waveguide effective index increases due to temperature rise caused by self-heating and the ring resonance wavelength red-shifts, the amount of which depends on the input optical power. Since Si MRM characteristics greatly depend on the ring resonance wavelength, self-heating can strongly influence the modulation performance and, consequently, its influence must be well understood and controlled in order to realize reliable and efficient depletion-type Si MRMs. For this, an accurate and easy-to-use model of Si MRM self-heating must be established.

In this paper, we investigate the influence of self-heating on transmission characteristics of depletion-type Si MRMs and provide an accurate model with the introduction of the self-heating coefficient, *R*, which can be easily measured and with which precise modeling of Si MRM static transmission characteristics at various input power levels can be realized. In addition, the dependence of *R* on MRM sizes and doping concentration are experimentally investigated and resulting dependencies are explained. This paper is organized in the following manner. In Section II, we briefly review the coupled-mode equation on which our modeling efforts are based. In Section III, we introduce the self-heating coefficient and demonstrate that Si MRM transmission characteristics can be precisely modeled. In Section IV, the dependence of *R* on device size and doping concentration are investigated. Section V concludes the paper.

II. Si MRM Model Based on Coupled Mode Equation

The dynamic behavior of a ring resonator can be modeled by the coupled mode equation as [6], [7]

$$\frac{d}{dt}a(t) = \left(j\omega_r - \frac{1}{\tau}\right)a(t) - j\mu E_i(t) \quad (1)$$

$$E_o(t) = E_i(t) - j\mu a(t). \quad (2)$$

In the above equation, $|a(t)|^2$ represents the optical energy stored in the ring resonator, $E_i(t)$ and $E_o(t)$ are the input and the output optical field, respectively. ω_r is the ring resonance angular frequency given as $\omega_r = \frac{2\pi m c}{n_{res} L}$, where m is an integer representing the resonance mode number, c is the velocity of light in vacuum, L is the ring circumference, and n_{res} is the effective index of the ring waveguide at the resonance. τ is the decay time constant for $a(t)$, and μ represents the change in $a(t)$ due to the input optical field. Assuming the Si MRM has large enough Q-factor, which is usually the case for high-performance Si MRMs, the parameters used in above equations are related to parameters for the more commonly used MRM round-trip

Manuscript received February 01, 2016; revised April 15, 2016; accepted April 23, 2016. This work was supported by the National Research Foundation of Korea funded by the Korean government under Grant 2015R1A2A2A01007772.

M.-J. Shin, B.-M. Yu, and W.-Y. Choi are with the Department of Electrical and Electronic Engineering, Yonsei University, Seoul 120-749, South Korea (e-mail: slayier55@gmail.com; dbqudals1989@gmail.com; wchoi@yonsei.ac.kr).

Y. Ban was with the Department of Electrical and Electronic Engineering, Yonsei University, Seoul 120-749, South Korea. He is now with the IMEC vzw, Heverlee B-3001, Belgium (e-mail: ryoojin0509@gmail.com).

J. Rhim was with the Department of Electrical and Electronic Engineering, Yonsei University, Seoul 120-749, South Korea. He is now with the Hewlett Packard Laboratories, Palo Alto, CA 94304 USA (e-mail:peterjinsoorhim@gmail.com).

L. Zimmermann is with the Innovations for High Performance Microelectronics, Brandenburg 15236, Germany (e-mail: lzimmermann@ihp-microelectronics.com).

Color versions of one or more of the figures in this paper are available online at http://ieeexplore.ieee.org.

Digital Object Identifier 10.1109/JSTQE.2016.2560149

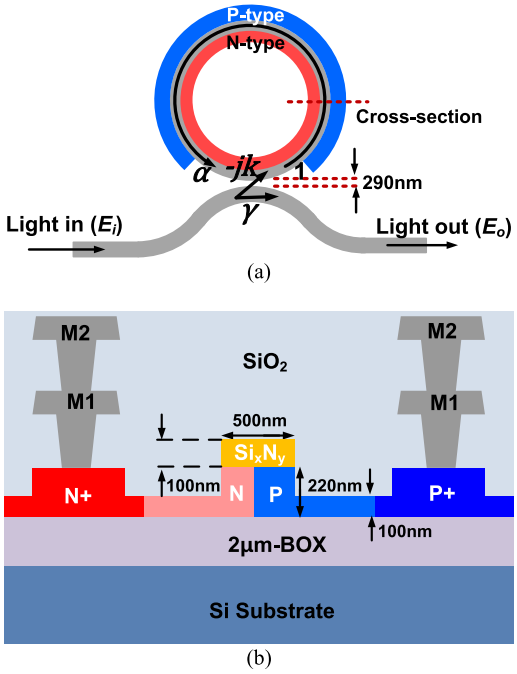

Fig. 1. (a) Structure and (b) cross-section of Si MRM.

model [8] in the following manner,

$$\frac{1}{\tau} = \frac{(2-\alpha^2-\gamma^2)c}{2nL} \tag{3}$$

$$\mu^2 = \frac{(1-\gamma^2)c}{nL}. \tag{4}$$

Here, α represents the field ratio after one round-trip in the ring waveguide and γ is the through coefficient in the directional coupler composed of ring and bus waveguides. These parameters are graphically represented in Fig. 1(a).

For $E_i(t)$ having *exp(jωt)* dependence, we can obtain the steady-state solution for $a(j\omega)$ as

$$a = \frac{-j\mu}{j(\omega-\omega_r)+\frac{1}{\tau}} E_i. \tag{5}$$

By substituting (5) into (2) we have

$$\left|\frac{E_o}{E_i}\right|^2 = \frac{(\omega-\omega_r)^2+\left(\frac{1}{\tau}-\mu^2\right)^2}{(\omega-\omega_r)^2+\frac{1}{\tau^2}}. \tag{6}$$

The numerical value for each parameter used in above equations can be determined by fitting (6) into the measured transmission spectrum. As an example, Fig. 2(a) and (b) show measured transmission spectra for a sample Si MRM. As shown in Fig. 1(b), the device has 220 nm thick Si waveguide above 2 μm thick buried oxide (BOX) layer and 500 nm wide ring and bus waveguides. The 100-nm thick Si_xN_y layer is used for definition of the rib waveguide core. The nominal ratio for N- and P-region widths is 2:3. All Si MRMs reported in this paper were fabricated through Si PIC MPW provided by IHP and have the same device structures except the ring radius, gap distance between ring and bus waveguides, and doping concentration. The

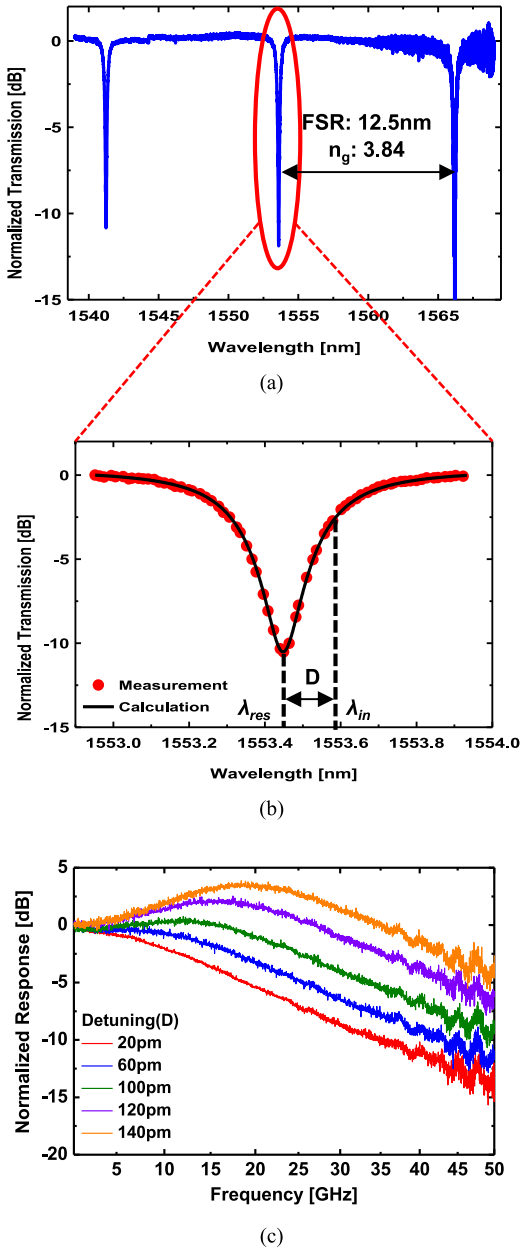

Fig. 2. (a) Measured broad transmission spectrum of Si MRM. (b) Measured and calculated transmission spectra without self-heating. For calculation, extracted parameters given in Table I are used. (c) Measured small-signal modulation characteristics at five different detuning values. It was measured with low input power where self-heating effect is negligible.

Si MRM device whose transmission spectrum is shown in Fig. 2 has ring radius of 8 μm, gap distance of 290 nm and nominal doping concentrations of 7×10^{17} (cm^{-3}) for P-region and 5×10^{18} (cm^{-3}) for N-region. An Er-doped fiber amplifier is used for the broadband transmission spectrum shown in Fig. 2(a), and a tunable laser for the narrow-band spectrum shown Fig. 2(b). The input optical power is reduced as much as possible in order to avoid any self-heating for these measurements. For the spectrum shown in Fig. 2(b), the optical power injected into the bus waveguide is estimated 0.025 mW after the coupling loss due to on-chip grating couplers are calibrated out. Si MRM devices

TABLE I
EXTRACTED SI MRM PARAMETERS

λ_{res} (nm)	m	n_{res}	$1/\tau$ (s^{-1}) (x10^{11})	u^2 (s^{-1}) (x10^{10})	α	γ
1553.449	86	2.657814	1.1351	8.0938	0.9669	0.9818

are placed on the probing stage whose temperature is actively controlled to be at 25 °C.

The transmission spectrum in Fig. 2(a) shows FSR of 12.5 nm, from which n_g, the group index, of 3.84 can be determined. Fig. 2(b) shows the measured (red circles) narrow-band transmission spectrum for one of the resonance peaks shown in Fig. 2(a) along with the calculated results (black line) using the extracted coupled-mode equation parameters. For parameter extraction, the integer value of *m*, representing the resonance mode number is determined from the numerical simulation of the ring waveguide and n_{res} is determined from the measured λ_{res} using $\lambda_{res} = \frac{L}{m} n_{res}$. Then, τ and u are determined by fitting (6) into the measured spectrum so that the minimum mean squared error is achieved. Fig. 2(b) shows that measurement and calculation results agree very well. Table I shows the extracted values for the coupled-mode equation parameters as well as converted round-trip model parameters for selected resonance peak. Although extraction is done for τ and *u*, α and γ are also used in this paper since they are more closely related to the device parameters and allow easier interpretation. Fig. 2(c) shows the measured modulation frequency responses of the same Si MRM at several different input wavelengths, which are detuned from the resonance wavelength by the amount (D) shown in the figure. The input optical power injected is 0.025 mW. The modulation frequency response of a Si MRM has been extensively investigated and there exist several models with which the peak values and the peaking frequency in the frequency response can be determined [9]–[11]. Although self-heating does not directly affect the modulation frequency responses since the time scale for self-heating is much larger than the modulation time scale of interest, self-heating strongly influences the resonance wavelength, which in turn affects the modulation frequency response [12] as shown in Fig. 2(c).

III. PARAMETRIC MODELING OF SELF-HEATING

As the input optical power becomes larger in the depletion-type Si MRM, the resonance wavelength shifts to longer wavelength and the transmission spectrum becomes asymmetric due to self-heating as shown in Fig. 3, which shows transmission spectra measured at two different input power levels of 0.025 and 1.000 mW for the sample Si MRM device mentioned above. Fig. 4(a) shows the measured resonance wavelength at different input powers for the same device. The red line in Fig. 4(b) is linearly fitted to changes in the effective refractive index of the ring waveguide for different input powers determined from $m\,\lambda_{res} = n_{res} L$, where λ_{res} and n_{res} represent the resonance wavelength and its effective index, and *m* is an integer. The change in the effective index is caused by temperature increase

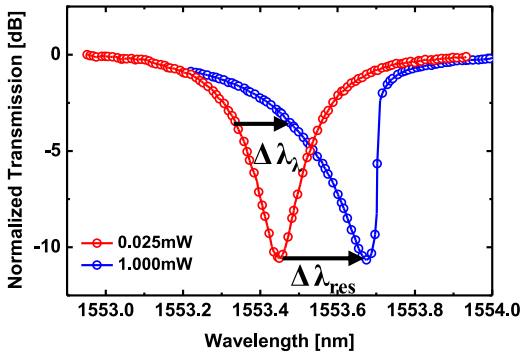

Fig. 3. Measured transmission spectra at two different input powers.

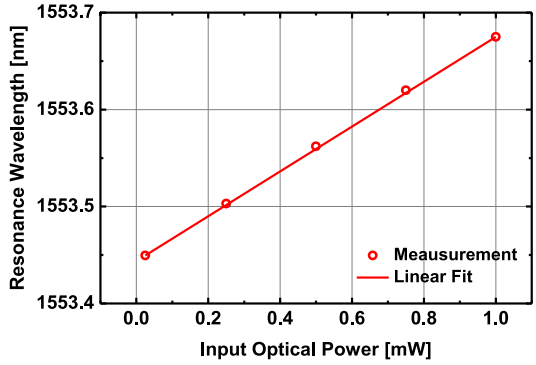

(a)

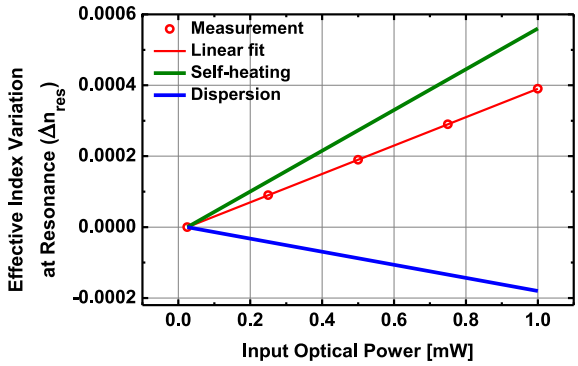

(b)

Fig. 4. (a) Measured resonance wavelength and (b) effective index variation at resonance wavelength at different input optical powers. Also shown in (b) are estimated effective index variation due to only temperature change and dispersion.

in the ring waveguide by self-heating as well as dispersion of the effective index. Or,

$$\Delta n_{res} = \frac{\delta n_{res}}{\delta T} \Delta T + \frac{\delta n_{res}}{\delta \lambda} \Delta \lambda_{res}. \tag{7}$$

The amount of resonance wavelength shift due to self-heating can be expressed as [13], [14]

$$\Delta \lambda_{res} = \lambda_{res} \frac{\Delta n_{res}}{n_{res}} = \frac{\lambda_{res}}{n_g} \frac{\delta n_{res}}{\delta T} \Delta T, \tag{8}$$

where $n_g = n_{res} - \lambda \frac{\delta n_{res}}{\delta \lambda}$. Since it is more convenient to express $\Delta\lambda_{res}$ as a function of input optical power, as it can be directly measured, we can rewrite (8) as

$$\Delta\lambda_{res} = \frac{\lambda_{res}}{n_g} R \Delta I_{in} \tag{9}$$

where ΔI_{in} is the input optical power change and *R* is a newly-introduced self-heating coefficient. By comparing (8) and (9), we have

$$R = \frac{\delta n_{res}}{\delta T} \frac{\Delta T}{\Delta I_{in}} \tag{10}$$

or *R* represents the change in n_{res} due to only temperature change caused by input power increase. As can be seen in (9), *R* can be easily determined by measuring the change in resonance wavelength caused by the input power change with the knowledge of the group index. For the Si MRM device measured for Fig. 4(a), $R = 5.67 \times 10^{-4}$ (/mW) can be determined using 3.84 for n_g. Since the resonance wavelength change is linear for the input power ranges of interest, measurements at two different input power levels should be sufficient for *R* determination. With this R, we can plot the green line in Fig. 4(b), which represents the effective index change due to temperature change. The difference between green and red lines in Fig. 4(b) is the effective index change due to dispersion, which is shown with a blue line in Fig. 4(b). Since the sign of dispersion for Si is negative, or Si refractive index decreases with wavelength increase [15], the influence of self-heating is somewhat reduced due to dispersion in Si MRMs.

The optical Kerr effect can also cause linear increase in the refractive index in Si with increasing optical power. However, we can easily rule this out for the present investigation since the observed index change is much larger than the amount possible with the optical Kerr effect. With Kerr coefficient of $n_2 = 3 \sim 6 \times 10^{-18} (\mathrm{m}^2/\mathrm{W})$ for Si [16], [17], the amount of refractive index change due to the Kerr effect in the Si waveguide in our MRM can be estimated much less than those observed in the present investigation. We can also estimate the actual temperature increase in the ring waveguide due to self-heating by approximating $\frac{\delta n_{eff}}{\delta T}$ with $\Gamma_{core} \frac{\delta n_{core}}{\delta T} + (1 - \Gamma_{core}) \frac{\delta n_{cladding}}{\delta T}$. Si has thermo-optical coefficient $\left(\frac{\delta n_{core}}{\delta T}\right)$ of 1.86×10^{-4}/K [14] and Γ_{core} can be determined to be about 0.72 from numerical simulation of the ring waveguide. $\frac{\delta n_{cladding}}{\delta T}$ can be approximated with thermo-optic coefficient of SiO_2, which is about 1×10^{-5}/K [14], [18]. Then, for Δn_{eff} of 5.67×10^{-4} due to self-heating with 1mW input power determined from Fig. 4(b), there is about 4.1° temperature increase in the ring waveguide.

The influence of self-heating on the transmission spectrum is recursive in that self-heating changes the resonance wavelength, which in turn changes the amount of self-heating at a given wavelength [19]. This makes it difficult to determine the exact transmission spectrum including self-heating. However, since the amount of red shift due to self-heating should be proportional to the optical power circulating in the ring waveguide for any wavelength near the resonance, we can determine the amount of red shift for any wavelength by the following linear approximation,

$$\Delta\lambda_{\lambda} \sim \Delta\lambda_{res} \frac{|A_{\lambda}|^2}{|A_{res}|^2} \tag{11}$$

where $|A_{\lambda}|^2$ represents the optical power inside the ring waveguide at λ near resonance. Fig. 3 shows clear definition for $\Delta\lambda_{\lambda}$ and $\Delta\lambda_{res}$. From the analysis based on the coupled-mode equation, $|A_{\lambda}|^2$ can be expressed as [7], [19]

$$|A_{\lambda}|^2 = |a_{\lambda}|^2 \frac{c}{nL}. \tag{12}$$

Assuming the value of *n* in (12) does not change much for the wavelength range of interest at a given input power, substituting (12) into (11), and using (5) for $|a_{\lambda}|^2$, we have

$$\Delta\lambda_{\lambda} \sim \Delta\lambda_{res} \frac{|a_{\lambda}|^2}{|a_{res}|^2} = \Delta\lambda_{res} \frac{(2 - \alpha^2 - \gamma^2)^2 c^2}{4 n_{res}^2 L^2 (\omega - \omega_r)^2 + (2 - \alpha^2 - \gamma^2)^2 c^2} \tag{13}$$

where all the parameters in the equation except $\Delta\lambda_{res}$ are MRM parameters determined at low input power without self-heating. In other words, if we measure the MRM transmission spectrum at low input power and the amount of resonance wavelength red-shift due to larger input power, we can determine transmission spectrum at that larger input power using (13).

Fig. 5(a) shows measured transmission spectra for selected resonance peak shown in Fig. 2(a) at five different input power levels and the calculated spectra using (13) with exacted parameters given in Table I and measured $\Delta\lambda_{res}$. As can be seen, they agree very well, confirming the accuracy of our model. At higher input optical powers, the transmission spectra show bi-stability, which is not consider for the present investigation as bi-stability is not desirable for applications we are interested in.

TABLE II
EXTRACTED PARAMETERS FOR SI MRMS HAVING DIFFERENT RADII

Radius (μm)	Gap (nm)	α	γ	R (/mW)	R ratio	$\lvert A_{res}\rvert^2$ ratio
8	290	0.9669	0.9818	5.67E–4	1.00	1.00
12	250	0.9507	0.9708	3.99E–4	0.70	0.69
16	220	0.9323	0.9523	2.96E–4	0.52	0.52

IV. DEPENDENCE OF R ON OPTICAL POWER IN THE RING AND DOPING CONCENTRATION

Fig. 5(a)–(c) show measured and calculated transmission spectra at different input power levels for three different Si MRM devices having different ring radii and gap distances between ring and bus waveguides. These devices have the same Si MRM structures except ring radius and gap distance. Table II shows the extracted parameters along with *R* and $|A_{res}|^2$ ratios normalized to the values for 8 um device. As can be shown in

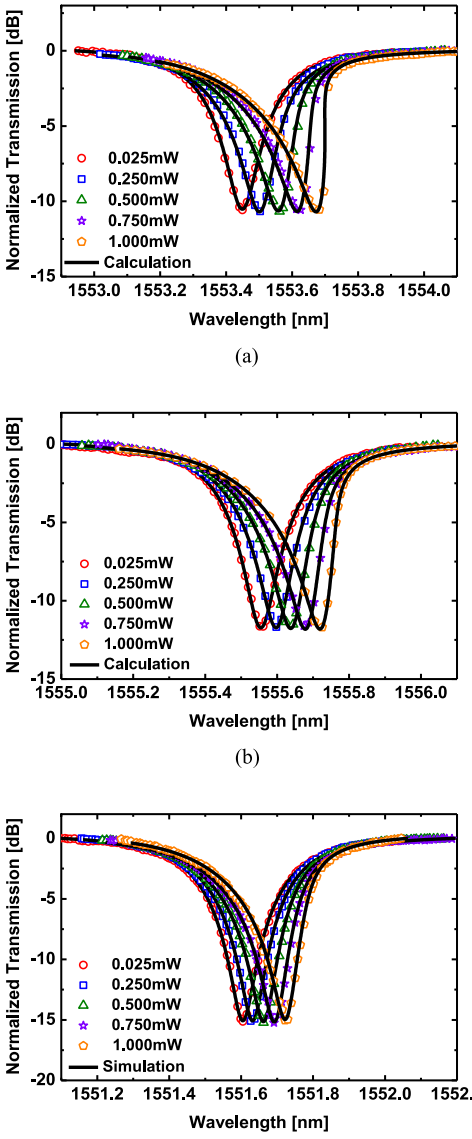

Fig. 5. Measured and calculated transmission spectra at different input optical powers for Si MRMs having different radii and directional coupler gap distances, 8 μm and 290 nm for (a), 12 μm and 250 nm for (b), and 16 μm and 220 nm for (c).

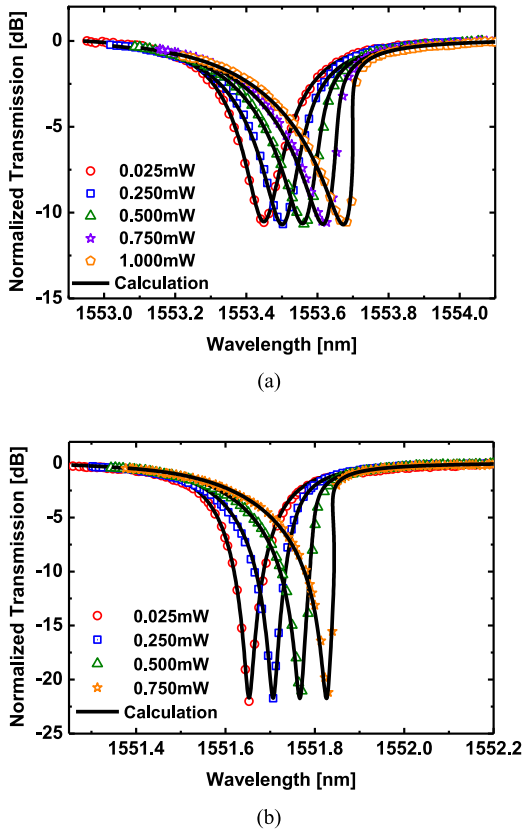

Fig. 6. Measured and calculated transmission spectra at different input optical powers for Si MRMs having different doping concentration, $7 \times 10^{17}(\mathrm{cm}^{-3})$, $5 \times 10^{18}(\mathrm{cm}^{-3})$ for P-, N-type for (a), $5 \times 10^{17}(\mathrm{cm}^{-3})$, $3 \times 10^{18}(\mathrm{cm}^{-3})$ for P-, N-type for (b). For (b), 1mW was not included where Si MRM shows bi-stability.

the table, R values differ for different devices. This difference can be explained by noting that $\frac{\Delta T}{\Delta I_{in}}$ in (10) can be further expanded as

$$\frac{\Delta T}{\Delta I_{in}} = \frac{\Delta T}{\Delta \left|A_{res}\right|^2} \cdot \frac{\Delta \left|A_{res}\right|^2}{\Delta I_{in}}. \tag{14}$$

Consequently, Si MRMs can have different R values due to the difference in $\left|A_{res}\right|^2$ caused by differences in α and γ. From (5) and (12), we can derive

$$\left|A_{res}\right|^2 = \frac{4(1-\gamma^2)}{(2-\alpha^2-\gamma^2)^2} \cdot I_{in} \tag{15}$$

which can be easily calculated using extracted model parameters. The calculated ratios for the optical powers in the ring waveguide at the resonance wavelength are shown in Table II. As can be seen, their ratios are almost identical to R ratios, indicating the difference in R values for these three Si MRMs are purely due to the different amount of the optical power inside the ring waveguide at the resonance.

Fig. 6(a), (b) show the measured and calculated transmission spectra at different input power levels for two Si MRM devices having different doping concentrations. Note that Fig. 6(a) is identical to Fig. 5(a), two Si MRM devices differ only their doping concentrations. Table III shows the extracted parameters along with R and $\left|\mathrm{A_{res}}\right|^2$ ratios normalized to the values for 8 um device. Even though the device with lower doping concentration has higher optical power inside the ring, both devices have similar R values. This is due to the doping concentration dependence of FCA [20], [21], which is related to $\frac{\Delta T}{\Delta \left|A_{res}\right|^2}$ in (14). This clearly shows that doping concentrations as well as device structures influence the amount of optical powers in the ring at the resonance. Consequently, these factors should be carefully considered in order to have clear understanding of self-heating.

TABLE III
EXTRACTED PARAMETERS FOR SI MRMS HAVING DIFFERENT DOPING CONCENTRATION

P/N Doping Concentration	α	γ	R /mW)	R ratio	$\lvert A_{res}\rvert^2$ ratio
P: $7 \times 10^{17}(cm^{-3}) : 5 \times 10^{18}(cm^{-3})$	0.9669	0.9818	5.67E–4	1	1.00
P: $5 \times 10^{17}(cm^{-3}) : 3 \times 10^{18}(cm^{-3})$	0.9801	0.9831	5.89E–4	1.04	1.79

V. CONCLUSION

We investigated the influence of self-heating on the transmission spectrum of the depletion-type Si MRM. FCA in the doped ring waveguide causes temperature rise and increases the effective index, which changes the resonance wavelength and the transmission spectrum. We introduced the self-heating coefficient (R), which can be easily measured and with which changes of the effective index at the resonance wavelength due to self-heating can be precisely modeled. Although it takes transmission spectrum measurements at two different optical input power levels for determining R, transmission spectra as well as the exact value of Si MRM resonance wavelength shift can be determined at any input power level with the knowledge of R as demonstrated in our paper. The accuracy of our model was confirmed by comparing measured transmission spectra for several different Si MRM devices with calculated spectra based on our model. In addition, we clarified the influence of device size and doping concentration on R. These results should provide useful guidelines for designing Si MRMs that suffer less from self-heating. Our self-heating model should be of great help for precisely understanding Si MRM characteristics and designing the optimal Si MRM for given applications.

REFERENCES

[1] R. Soref, "The past, present, and future of silicon photonics," *IEEE J. Sel. Topics Quantum Electron.*, vol. 12, no. 6, pp. 1678–1687, Nov./Dec. 2006.

[2] Q. Xu, B. Schmidt, S. Pradhan, and M. Lipson, "Micrometre-scale silicon electro-optic modulator," *Nature*, vol. 435, pp. 325–327, 2005.

[3] T. Baba *et al.*, "50-Gb/s ring-resonator-based silicon modulator," *Opt. Express*, vol. 21, no. 10, pp. 11869–11876, 2013.

[4] X. Xiao *et al.*, "44Gb/s silicon microring modulators based on zigzag PN junctions," *IEEE Photon. Technol. Lett.*, vol. 24, no. 19, pp. 1712–1714, Oct. 2012.

[5] X. Zheng *et al.*, "Enhanced optical bistability from self-heating due to free carrier absorption in substrate removed silicon ring modulators," *Opt. Express*, vol. 20, no. 10, pp. 11478–11486, 2012.

[6] H. A. Haus, "Coupling of modes -resonators and couplers," in *Waves and Fields in Optoelectronics*. Englewood Cliffs, NJ, USA: Prentic-Hall, 1984, p. 07632.

[7] B. E. Little, S. T. Chu, H. A. Haus, J. S. Foresi, and J.-P. Laine, "Microring resonator channel dropping filter," *J. Lightw. Technol.*, vol. 15, no. 6, pp. 998–1005, Jun. 1997.

[8] W. Bogaerts *et al.*, "Silicon microring resonator," *Laser Photon. Rev.*, vol. 6, no. 1, pp. 47–73, 2012.

[9] B. Pile and G. Taylor, "Small-signal analysis of microring resonator modulator," *Opt. Express*, vol. 22, no. 12, pp. 14913–14928, 2014.

[10] Y. Ban, J.-M. Lee, B.-M. Yu, S.-H. Cho, and W.-Y. Choi, "Small-signal frequency responses for Si micro-ring modulator," in *Proc. IEEE Optical Interconnects Conf.*, 2014, pp. 47–48.

[11] J. Müller *et al.*, "Optical peaking enhancement in high-speed ring modulators," *Scientific Rep.*, vol. 4, no. 6310, pp. 1–9, 2014.

[12] W. D. Sacher and J. K. S. Poon, "Dynamics of microring resonator modulators," *Opt. Express*, vol. 16, no. 20, pp. 15741–15753, 2008.

[13] Q. Fang *et al.*, "High efficient ring-resonator filter with NiSi heater," *IEEE Photon. Technol. Lett.*, vol. 24, no. 5, pp. 350–352, Mar. 2012.

[14] K. Padmaraju and K. Bergman, "Resolving the thermal challenges for silicon microring resonator devices," *Nanophotonics*, vol. 3, no. 4/5, pp. 269–281, 2014.

[15] B. J. Frey, D. B. Leviton, and T. J. Madison, "Temperature-dependent refractive index of silicon and germanium," *Proc. SPIE*, vol. 6273, pp. 62732J–1–62732J-10, 2006.

[16] H. K. Tsang and Y. Liu, "Nonlinear optical properties of silicon waveguides," *Semicond. Sci. Technol.*, vol. 23, no. 6, pp. 064007-1–064007-9, 2008

[17] J. Leuthold, C. Koos, and W. Freude, "Nonlinear silicon photonics," *Nature Photon.*, vol. 4, pp. 535–544, 2010.

[18] A. Arbabi and L. L. Goddard, "Measurements of the refractive indices and thermos-optic coefficients of Si_3N_4 and SiO_x using microring resonaces," *Opt. Lett.*, vol. 38, no. 19, pp. 3878–3881, 2013.

[19] Y. Ban, B. M. Yu, J. Rhim, J. M. Lee and W. Y. Choi, "Modeling of self-heating effect for depletion-type Si micro-ring modulator," in *Proc. IEEE Opt. Interconnects Conf.*, 2015. [Online]. Available: http://ieeexplore.ieee.org/xpl/articleDetails.jsp?reload = true&arnumb er = 7115722

[20] D. K. Schroder, R. N. Tomas, and J. C. Swartz, "Free carrier absorption in silicon," *IEEE J. Solid-Sate Circuits*, vol. 13, no. 1, pp. 180–187, Feb. 1978.

[21] R. A. Soref and B. R. Bennett, "Electrooptical effects in silicon," *IEEE J. Quantum Electron.*, vol. 23, no. 1, pp. 123–129, Jan. 1987.

Myung Jin Shin received the B.S degree in electrical and electronic engineering from Yonsei University, Seoul, South Korea, in 2015. where he is currently working toward the M.S. degree at the same university. His research interests include design, modeling, and optimization of Si-based electronic-photonic integrated circuits.

Yoojin Ban received the B.S. and M.S. degrees in electrical and electronic engineering from Yonsei University, Seoul, South Korea, in 2013 and 2015, respectively. Her M.S. thesis was on silicon microring modulator modeling. In 2015, she joined IMEC in Belgium as a Researcher. Her research interests include high speed and efficient modulators based on silicon photonics.

Byung-Min Yu received the B.S. degree in electrical and electronic engineering from Yonsei University, Seoul, South Korea, in 2012. He is currently working toward the Ph.D. degree at the same university. His research interests include design, modeling, and optimization of silicon photonic devices.

Jinsoo Rhim received the B.S. and Ph.D. degrees in electrical and electronic engineering from Yonsei University, Seoul, South Korea, in 2009 and 2016, respectively. His doctoral dissertation concerned modeling, design, and optimization of Si photonic transmitters. In 2016, he joined Hewlett Packard Laboratories, Palo Alto, USA. His research interests include photonic device characterization and modeling, Si-based electronic-photonic IC design, and high-speed interface circuit design in advanced CMOS/BiCMOS technology.

Lars Zimmermann received the Graduate degree from Friedrich Schiller University in Jena, Jena, Germany, and Technische Universitaet Delft in The Netherlands, Delft, The Netherlands. He received the Ph.D. degree in electrical engineering from Katholieke Universiteit Leuven, Leuven, Belgium, for his work on near-infrared sensor arrays that he conducted at IMEC. He moved to Technische Universitaet Berlin in 2004, where he worked on integrated optics and hybrid integration. After joining IHP, Frankfurt (Oder), Germany in 2008, he is currently a Team Leader of Silicon Photonics Technologies. His current work is dedicated to photonic building blocks and high-performance photonicelectronic integration for optical communications, for photonic-electronic convergence, and for nonlinear optical signal processing. He is also with TU Berlin, Berlin, Germany, coordinating the cooperation with IHP in the field of silicon photonics.

Woo-Young Choi (M'92) received the B.S., M.S., and Ph.D. degrees in electrical engineering and computer science from the Massachusetts Institute of Technology, Cambridge, MA, USA, in 1986, 1988, and 1994, respectively. His doctoral dissertation concerned the investigation of molecular-beam epitaxy-grown InGaAlAs laser diodes for fiber-optic applications. From 1994 to 1995, he was a Postdoctoral Research Fellow at NTT Opto-Electronics Laboratories, where he worked on femtosecond all-optical switching devices based on low-temperature grown InGaAlAs quantum wells. In 1995, he joined the Department of Electrical and Electronic Engineering, Yonsei University, Seoul, South Korea, where he is currently a Professor. His research interests include high-speed circuits and systems that include high-speed optoelectronics, high-speed electronic circuits, and silicon photonics.